



Published in final edited form as:

Biochemistry. 2011 August 16; 50(32): 6879–6887. doi:10.1021/bi2007299.

Kinetic and Chemical Mechanism of Malate Synthase from *Mycobacterium tuberculosis*

Christine E. Quartararo[‡] and John S. Blanchard^{‡,*}

[‡]Department of Biochemistry, Albert Einstein College of Medicine, 1300 Morris Park Avenue, Bronx, New York 10461

Abstract

Malate synthase catalyzes the Claisen-like condensation of acetyl-coenzyme A and glyoxylate in the glyoxylate shunt of the citric acid cycle. The *Mycobacterium tuberculosis* malate synthase G gene, *glcB*, was cloned, and the N-terminal His₆ tagged 80 kDa protein was expressed in soluble form and purified by metal affinity chromatography. A chromogenic 4,4'-dithiodipyridine assay did not yield linear kinetics, but the generation of an active site directed mutant, C619S, gave an active enzyme and linear kinetics. The resulting mutant exhibited comparable kinetics to wild type and was used for the full kinetic analysis. Initial velocity studies were intersecting suggesting a sequential mechanism, which was confirmed by product and dead-end inhibition. The inhibition studies delineated the ordered binding of glyoxylate followed by AcCoA and the ordered release of CoA followed by malate. The pH dependence of k_{cat} and k_{cat}/K_{gly} are both bell-shaped and catalysis depends on a general base (pK 5.3) and a general acid (pK 9.2). Primary kinetic isotope effects determined using [C²H₃-methyl] acetyl-CoA suggested that proton removal and carbon-carbon bond formation were partially rate-limiting. Solvent kinetic isotope effects on k_{cat} suggested the hydrolysis of the malyl-CoA intermediate was also partially rate-limiting. Multiple kinetic isotope effects, utilizing D₂O and [C²H₃-methyl] acetyl-CoA, confirmed a stepwise mechanism in which the step exhibiting primary kinetic isotope effects precedes the step exhibiting the solvent isotope effects. The kinetic data and the pH dependence of the kinetic parameters were combined with existing structural and mutagenesis data to propose a chemical mechanism for malate synthase from *Mycobacterium tuberculosis*.

Keywords

malate synthase; glyoxylate shunt; kinetics; isotope effects; tuberculosis

Malate synthase (MS) is an enzyme in the glyoxylate shunt of the citric acid cycle in a wide range of pro- and eukaryotes. The glyoxylate shunt has been implicated in the pathogenesis of several bacteria and fungi (1), is not present in placental mammals (2), and therefore represents an attractive drug target. The anaplerotic shunt allows for the assimilation of acetyl-coenzyme A (AcCoA) from fatty acid oxidation or *de novo* synthesis. By bypassing the two decarboxylative steps of the TCA cycle, respiration can continue when only two carbon substrates such as acetate or ethanol are available. The first reaction of the glyoxylate shunt occurs by the action of isocitrate lyase to convert isocitrate to succinate and

*To whom correspondence should be addressed: Department of Biochemistry, Albert Einstein College of Medicine, 1300 Morris Park Ave., Bronx, NY 10461. Phone: (718) 430–3096. Fax: (718) 430–8565. blanchar@aecom.yu.edu.

SUPPORTING INFORMATION

Figure S1, a time course comparison of WT MS and C619S MS activity, can be found in the supporting information. Supplemental materials may be accessed free of charge online at <http://pubs.acs.org>.

glyoxylate. Malate synthase then catalyzes the Claisen-like condensation of glyoxylate and AcCoA to malate and coenzyme A (CoA).

The mechanism by which *Mycobacterium tuberculosis* (Mtb) enters into a non-replicating, persistent state has been probed by the *in vitro* Wayne Model (3). In the Wayne model, Mtb bacilli gradually consume the available oxygen and survive in a non-replicating persistence state under these low oxygen conditions. The hypoxic environment is thought to be similar to that inside the granulomatous lesions that Mtb resides during latency. Under these conditions there is an increase in the production of isocitrate lyase and glycine dehydrogenase, which generates glycine from glyoxylate (4). Disruption of the isocitrate lyase gene has shown the necessity of the glyoxylate shunt in the survival of persistent Mtb (5), establishing the physiological significance of this shunt in the persistence of Mtb. Mtb is a global health epidemic in which there were 9.4 million new cases in 2009 (6). Of these new infections, 60–90% will develop latent infection (7), which is not yet targetable by any therapy. Furthermore, multiple and extensively drug resistant stains (MDR and XDR) have emerged, creating a dire need for novel drug targets.

Claisen condensation enzymes catalyze biosynthetic carbon-carbon bond formation typically in the elongation reactions of fatty acid or polyketide synthesis (8). However MS operates in the TCA cycle, catalyzing a Claisen-like condensation outside of these realms. Similar enzymes, which catalyze Claisen-like condensations outside of fatty acid and polyketide synthesis have been kinetically characterized and are available for comparison: citrate synthase (CS) also in the TCA cycle, α -isopropylmalate synthase (α -IPMS) in leucine biosynthesis, and homocitrate synthase (HCS) in lysine biosynthesis. Each of these enzymes uses an AcCoA derived carbon nucleophile and an alpha carbonyl-containing carboxylic acid substrate to create a CoA intermediate that is hydrolyzed to release product and CoA (9–11). MS, α -IPMS, and HCS, are all dependent on a divalent metal (10, 12, 13), while CS utilizes two active site histidine residues (14).

In this paper we report the use of a characterized malate synthase mutant amenable to a continuous, chromogenic 4,4'-dithiodipyridine (DTP) assay. Initial velocity studies, dead-end and product inhibition determined the steady-state ordered bi bi kinetic mechanism for substrate binding and product release. The pH dependence of the kinetic parameters, primary kinetic isotope effects, and solvent kinetic isotope effects were determined. Previously, the structure of malate synthase from Mtb was determined in complex with the metal cofactor Mg^{2+} , and both substrate glyoxylate (PDB ID 1N8I) and products CoA and malate (PDB ID 1N8W) (13). The primary sequence, predetermined structural data, and newly presented kinetic data provide the basis for a proposed chemical mechanism.

MATERIALS AND METHODS

Materials

All chemicals were purchased from Sigma Aldrich. The pET-28a(+) vector was from Novagen, cloning enzymes and T7 express competent *Escherichia coli* (*E. coli*) cells were from New England Biolabs, and primers were from Invitrogen. DNase and Complete EDTA-free Protease were from Roche. 99.9% deuterated water was from Cambridge Isotope Laboratories.

Cloning, Overexpression, and Purification of MS

The Mtb *glcB* gene (Rv1837c) was PCR amplified from H37Rv DNA using the forward primer 5'-ATCCCGCTCATATGACAGATCGCGTGTCTGGTG-3' and reverse primer 5'-ATCCCGCTCTCGAGCTAGCGGGCCGCATCGTCACC-3'. Restriction sites for NdeI and XhoI are underlined respectively. The PCR fragment was cloned into a pET-28a(+)

vector containing a N-terminal His₆-Tag. After sequence verification, the recombinant plasmid was transformed into T7 express competent cells. 6 L LB containing 30 µg/mL kanamycin were inoculated with 3 mL overnight starter culture and incubated at 37°C. At an A₆₀₀ ~ 0.6 – 0.8, cells were induced with 0.5 mM IPTG and incubated at 20°C overnight. Cells were harvested by centrifugation, and the pellets were resuspended in 50 mM Tris, pH 8.0 containing 400 mM NaCl, and 5% glycerol (Buffer A), then sonicated and centrifuged at 17,000 RPM for 35 min. to remove cellular debris. Batch purification was performed with a Ni-NTA agarose column. The column was washed with Buffer A and the protein was eluted with 350 mM imidazole in Buffer A. The His₆-Tag was removed by thrombin cleavage in 50 mM Tris containing 50 mM NaCl, 5% glycerol, 400 units of thrombin, 1 mM DDT, and 1 mM CaCl₂. After cleavage, the protein was dialyzed and stored in 50 mM Tris, pH 7.0 containing 50 mM NaCl at –20°C.

C619S MS Mutant

C619S MS was prepared using the QuikChange II Site-Directed Mutagenesis Kit and standard PCR modifications with the forward primer 5'-GTTGATCAAGGTGTCGGCTCATCGAAGGTGCCCGACATC-3' and the reverse primer 5'-GATGTCGGGCACCTTCGATGAGCCGACACCTTGATCAAC-3', where the mutated codon is underlined. Expression of the mutant plasmid followed the same protocol as the wild type, except with induction by 1 mM IPTG. The mutant was purified as above with the following modifications. Buffer A became 50 mM Tris, pH 8.0 containing 250 mM NaCl. One tablet Complete EDTA-free protease inhibitor mix, 250 µg DNAase, and 10 mM MgCl₂ were added to the pellets resuspended in 75 mL Buffer A before sonication. After similar batch purification, dialysis was performed to remove the His₆-Tag in 20 mM Tris, pH 8.4 containing 150 mM NaCl, 5% glycerol, 400 units of thrombin, 1 mM DDT and 1 mM CaCl₂. After dialysis the protein was then applied to a Superdex200 HiLoad 26/60 size exclusion column using a buffer of 50 mM HEPES, pH 7.0 containing 150 mM NaCl, 5% glycerol, pH 7.0 at a flow rate of 1 mL/min. Malate synthase containing fractions determined by SDS-PAGE were combined and judged to be ~95% pure. 15 µM aliquots were stored in 50 mM HEPES, pH 7.0 containing 150 mM NaCl, 25 mM MgCl₂ and 55% glycerol at –20°C.

Protein Concentration

The concentration of WT MS was determined using the Bio-Rad protein assay using bovine serum albumin as a standard. The concentration of C619S MS was determined using A₂₈₀ and an extinction coefficient, 79,000 M⁻¹cm⁻¹ (15, 16).

Measurement of Enzymatic Activity

Enzymatic activity was determined by a coupled 4,4'-dithiodipyridine (DTP) assay at 324 nm. Reactions were carried out in 50 mM HEPES, pH 7.5 containing 15 mM MgCl₂ and 200 µM DTP, substrates AcCoA and glyoxylate, to a final volume of 1 mL. All assays were performed at 25°C and 1.5 nM WT or C619S MS was added to initiate the reaction. Reactions were monitored spectrophotometrically until 10% substrate conversion to product. Rates were calculated using the molar extinction coefficient of DTP, 19,800 M⁻¹cm⁻¹ and the total enzyme concentration (E_T).

Data Fitting

All data fitting was performed with GraphPad Prism version 5.0d. In all graphs the points are the mean of experimental duplicates, and the error bars are the standard deviation. The solid lines are the result of fitting to the denoted equation.

Initial Velocity of WT and C619S MS

Initial kinetic parameters were estimated by saturating with one substrate and varying the concentration of the other substrate. The resulting curve was fit to eq 1 where V is the maximal velocity and S is the concentration of the varied substrate.

$$v=VS/(K_m+S) \quad (1)$$

Initial velocity studies were conducted at fixed, saturating concentrations of glyoxylate and varying concentrations of AcCoA and vice versa. The resulting patterns were fit globally to eq 2 for a sequential kinetic mechanism where V is the maximal velocity, A and B are the substrate concentrations, K_a and K_b are the respective Michaelis constants for each substrate, and K_{ia} is the inhibition constant for substrate A.

$$v=VAB/(K_{ia}K_b+K_aB+K_bA+AB) \quad (2)$$

pH Dependence of C619S MS Activity

The pH dependence of the kinetic parameters were determined in 50 mM buffer at the desired pH; Sodium Acetate pH 4.5–5.0, MES pH 5.0–6.5, HEPES pH 6.5–8.0, TAPS pH 8.0–10.0, at saturating conditions of AcCoA and varying concentrations of glyoxylate. The resulting k_{cat} and k_{cat}/K_{gly} data were fit to eq 3, which describes a bell-shaped curve to obtain both the pK_a , the negative log of the acid dissociation constant, and pK_b , the negative log of the base dissociation constant, where c is the pH independent plateau value.

$$\log k_{cat} \text{ or } \log k_{cat}/K_{gly} = \log (-c/(1+((K_b)/(10^{\wedge} - pH))+((10^{\wedge} - pH)/K_a))) \quad (3)$$

Dead-end and Product Inhibition

The dead-end inhibitor, dethio-CoA, was synthesized as previously described (17). It was purified on a Synergi Fusion-RP column (250 × 10.0 mm, Phenomenex) using a linear gradient of Buffer A, 0.2% trifluoroacetic acid in water and Buffer B, 0.2% trifluoroacetic acid in acetonitrile. Fractions having A_{260} that eluted with the same retention time were pooled and lyophilized overnight. Mass spectrometry was used to confirm the presence of dethio-CoA. The samples were stored in H_2O at $-20^{\circ}C$. Product inhibition by malate and dead-end inhibition by dethio-CoA were tested with variable amounts of inhibitor, and both varying concentrations of AcCoA and glyoxylate. Data was globally fit to eq 4 for competitive inhibition, eq 5 for uncompetitive inhibition, or eq 6 for noncompetitive inhibition, where S is the varied substrate concentration, I is inhibitor concentration, K_{is} is the inhibition constant for the slope, K_{ii} is the inhibition constant for the intercept, and K_m is the Michaelis constant of substrate S .

$$v=VS/(K_m(1+I/K_{is})+S) \quad (4)$$

$$v=VS/(K_m+S(1+I/K_{ii})) \quad (5)$$

$$v = VS / (K_m (1 + I/K_{is}) + S (1 + I/K_{ii})) \quad (6)$$

Kinetic Isotope Effects

Synthesis of [C^2H_3 -methyl] AcCoA was carried out by acetylation of coenzyme A (18) with excess deuterated acetic anhydride $(CD_3CO)_2O$. The CoA was dissolved in D_2O and combined with 5 mL anhydrous N,N -dimethylformamide and 10 μ L triethylamine (TEA). The mixture was stirred for 10 min. at 25°C. Deuterated acetic anhydride was added to 2 mL DMF and added drop wise to the stirring mixture. The purification, mass spectrometric identification, and storage were identical to that for dethio-CoA. Assays were performed with saturating conditions of glyoxylate and varying concentrations of AcCoA and [C^2H_3 -methyl] AcCoA. The results were globally fit to eq 7 where V is the maximal velocity, S is the concentration of AcCoA or [C^2H_3 -methyl] AcCoA, F_i is the fraction of isotope (0 or 1), $E_{V/K}$ is the effect on $(k_{cat}/K_m) - 1$ and E_V is the effect on $k_{cat} - 1$.

$$v = VS / (K (1 + F_i E_{V/K}) + S (1 + F_i E_V)) \quad (7)$$

The pH dependence of the KIEs was measured at pH 5.5 and 6.5 (MES), 7.5 (HEPES), and 8.5 and 9.5 (TAPS).

Solvent Kinetic Isotope Effects

Solvent kinetic isotope effects were measured with saturating concentrations of glyoxylate and varying concentrations of AcCoA, and globally fit to eq 7 where $F_i = 0$ for H_2O and $F_i = 0.93$ for D_2O . A viscosity control of 9% glycerol (19) did not show any effect on either V or V/K_{AcCoA} . A proton inventory was performed at saturating conditions of both AcCoA and glyoxylate at 10% increments from 0–90% D_2O .

Multiple Kinetic Isotope Effects

MKIEs were measured with saturating concentrations of glyoxylate and varying concentrations of [C^2H_3 -methyl] AcCoA in H_2O and 93% D_2O , and varying concentrations of AcCoA and [C^2H_3 -methyl] AcCoA in 93% D_2O . Data was globally fit to eq 7.

RESULTS AND DISCUSSION

Cloning, Expression, and Purification

For WT MS, PCR amplification of the *glcB* gene resulted in a single fragment, 2.2 kb, of the expected size, that sequencing confirmed lacked any mutation introduced by PCR. The C619S mutant form of MS was similarly sequenced to confirm only the designed mutation. Overexpression yielded soluble proteins of the expected mass, 80 kDa. Approximately 14 mg of pure WT MS and 22 mg of pure C619S MS were obtained per liter of culture. SDS-PAGE was used to determine the molecular mass, and > 90% purity.

Measurement of Enzyme Activity

WT MS failed to display linear kinetics above pH 7.0 using the DTP assay (Figure S1). The activity of WT MS was confirmed by directly monitoring thioester cleavage of substrate AcCoA by the decrease in absorbance at 232 nm between pH 4.8 – 8.5 (data not shown). A close examination of the crystallographically determined structure of Mtb MS (1N8I) (13) showed Cys619 to be near the active site. Site directed mutagenesis was used to produce C619S, which was active using a DTP assay and displayed linear kinetic traces from pH 4.5

– 10. A lag phase was observed, but the addition of 15 mM MgCl₂ to the storage buffer and 30 mM MgCl₂ to the reaction mixture caused the lag to disappear. The similarity of the kinetic constants obtained with the WT and C619S mutant suggested that the C619S mutant could be used to continue kinetic evaluation using the more sensitive and robust DTP assay. All further data reported are for C619S MS.

Kinetic Mechanism

Initial velocity studies were performed to distinguish between a sequential and a ping-pong mechanism. When varying glyoxylate at fixed AcCoA concentrations and fit to a sequential mechanism (Figure 1A), the following parameters were determined: $k_{\text{cat}} = 23 \pm 3 \text{ sec}^{-1}$, $K_{\text{gly}} = 30 \pm 6 \mu\text{M}$, $K_{\text{AcCoA}} = 10 \pm 3 \mu\text{M}$, $K_{\text{ia}} = 3 \pm 2 \mu\text{M}$. When varying AcCoA at fixed glyoxylate concentrations, a similar intersecting pattern was observed and the fit to a sequential mechanism (Figure 1B) yielded similar kinetic parameters. Based on the observed intersecting lines in both double-reciprocal plots (Figure 1A–B) a steady-state ordered mechanism is proposed.

Product and dead-end inhibition studies were performed to determine the order of substrate binding and product release. Product inhibition with malate was competitive against glyoxylate (Figure 1C) and noncompetitive against AcCoA (Figure 1D) suggesting that glyoxylate binds first and malate is released last, supporting an ordered kinetic mechanism. Dead-end inhibition by dethio-CoA was uncompetitive versus glyoxylate (Figure 1E), and competitive versus AcCoA (Figure 1F) suggesting that the dead-end inhibitor dethio-CoA binds to a different enzyme form than glyoxylate and to the same enzyme form as AcCoA. Together with the product inhibition results, the formation of an enzyme-glyoxylate complex is expected before the AcCoA can bind to create the ternary complex. The proposed kinetic mechanism is shown in Scheme 1 in which the ordered binding of glyoxylate is followed by AcCoA, CoA is released first, and malate is released last.

Studies in the yeast enzyme (20) proposed a sequential random kinetic mechanism, on the basis of the initial velocity double reciprocal plots intersecting on the x-axis at $-1/K_m$, indicating that the binding of one substrate is not affected by the binding of the other substrate. This initial velocity pattern was not observed in Mtb MS, and the Mtb MS inhibition studies also support an ordered, not random, kinetic mechanism. Mtb α -isopropylmalate synthase displays an intersecting initial velocity pattern, proceeding by a random kinetic mechanism (9). Homocitrate synthase and citrate synthase both exhibit ordered binding, with their respective non-AcCoA substrates, α -ketoglutarate and oxaloacetate, binding first (10, 11).

pH dependence of C619S MS Activity

To probe the chemical mechanism of MS, the pH dependencies of k_{cat} and $k_{\text{cat}}/K_{\text{gly}}$ (Figure 2) were examined between pH 4.5 and 10.0 to determine the protonation states of enzyme and substrates necessary for binding and catalysis. The pH-rate profile was determined using saturating conditions of AcCoA and varying concentrations of glyoxylate, but control points were added to confirm the same bell-shaped dependence of $\log k_{\text{cat}}$ when varying AcCoA. These points were not included during fitting to eq 3. A bell-shaped curve was observed for $\log k_{\text{cat}}$, with a group that must be deprotonated for catalysis exhibiting a $\text{p}K_a$ value of 5.3 ± 0.1 , and a group that must be protonated for catalysis exhibiting a $\text{p}K_b$ value of 9.2 ± 0.1 . The pH dependence of $\log k_{\text{cat}}/K_{\text{gly}}$ reports on ionizable groups responsible for binding and catalysis and was also bell-shaped ($\text{p}K_a = 4.6 \pm 0.2$ and $\text{p}K_b = 9.1 \pm 0.3$). A similar bell-shaped pH-rate profile was seen for $\log k_{\text{cat}}$ and $\log k_{\text{cat}}/K_m$ for both substrates of homocitrate synthase; evidence of acid-base catalysis (21). Based on crystal structures of *M. tuberculosis* (13) and mutagenesis studies (22), Asp633 is proposed to be the catalytic base

corresponding to $pK_a = 5.3 \pm 0.1$ in $\log k_{cat}$ and Arg339 is proposed to be the catalytic acid corresponding to $pK_b = 9.2 \pm 0.1$ in $\log k_{cat}$. The mutagenesis studies were done on the *E. coli* enzyme, but the primary sequences of the *E. coli* and the Mtb malate synthases are 58% identical and 74% similar. Additionally, superimposition of crystal structures Mtb 1N8W (13) and *E. coli* 1D8C (23) revealed nearly identical active sites, and the superimposable location of Mtb MS residues Asp633 and Arg339 and the corresponding *E. coli* residues.

Kinetic Isotope Effects

Primary kinetic isotope effects were measured at pH 7.5, determining ^{D}V and $^{D}V/K_{AcCoA}$ with AcCoA and $[C^2H_3\text{-methyl}]$ AcCoA (Figure 3A). Normal primary kinetic isotope effects were observed with $^{D}V = 1.4 \pm 0.1$ and $^{D}V/K_{AcCoA} = 2.3 \pm 0.3$, thus confirming that proton abstraction from the AcCoA methyl group is at least partially rate limiting. The unusual observation that $^{D}V/K_{AcCoA} > ^{D}V$ suggests that AcCoA is not sticky and there is a step after proton abstraction that is also partly rate-limiting, lowering ^{D}V . However, since ^{D}V is not unity it is unlikely that product release is substantially rate-limiting.

The primary KIEs from pH 5.5 – 9.5 were found to be independent of pH (Figure 3B) and therefore the proton abstraction from the AcCoA methyl group is rate limiting across all determined pH values. Primary KIEs using $[C^2H_3\text{-methyl}]$ AcCoA have been previously reported for the yeast enzyme to exhibit normal isotope effects on both V and V/K (1.3 ± 0.1) (24) and 1.37 for both V and V/K (20).

Solvent kinetic isotope effects were examined in 93% D_2O at pH 7.5, a region where the kinetic parameters are insensitive to small changes in pH (Figure 4A). There was no observed SKIE on $^{D2O}V/K_{AcCoA}$, but a normal effect on $^{D2O}V = 1.7 \pm 0.1$. This normal solvent kinetic isotope effect on V suggests that a step in catalysis is sensitive to solvent isotopic composition. We suggest that the ^{D2O}V isotope effect reports on the proton abstraction from the metal-bound water that initiates the hydrolysis of the malyl-CoA intermediate. The lack of a solvent effect on V/K_{AcCoA} suggests the step that is sensitive to solvent isotopic composition is not the same step as the deprotonation of AcCoA responsible for the primary kinetic isotope effect. Further, it argues that upon attack of the resonance stabilized AcCoA anion on metal-bound glyoxylate the resulting malyl-CoA exists as the alkoxide form. Finally, the unitary value of $^{D2O}V/K_{AcCoA}$ also argues for the chemically reasonable order of carbon-carbon bond formation preceding hydrolysis.

In a proton inventory experiment (Figure 4B) H_2O_V/D_2O_V was determined in 10% increments from 0–90% D_2O . A linear proton inventory is indicative of a single solvent-derived proton involved in the step that is solvent sensitive. While a linear fit is shown, the possibility of a slight curvilinear dependence, corresponding to more than one proton being “in flight” was recognized. In extrapolating the data to 100% D_2O , we obtained a value of 1.6, within error of the experimentally determined $^{D2O}V = 1.7 \pm 0.1$.

Multiple kinetic isotope effects were determined in two ways. In the first, the primary kinetic isotope effect was determined in 93% D_2O . As seen in Figure 4C, the magnitude of both $^{D}V/K_{AcCoA}$ and ^{D}V were reduced compared to their values in H_2O [$^{D}V/K_{AcCoA} = 1.5 \pm 0.3$ (D_2O) vs. 2.3 ± 0.3 (H_2O) and $^{D}V = 1.1 \pm 0.3$ (D_2O) vs. 1.4 ± 0.1 (H_2O)]. These data are most consistent with a stepwise mechanism (25) where the carbon-carbon bond formation and thioester hydrolysis occur in two separate steps. The sequential nature of the two chemical steps are also supported by the earlier findings where $^{D}V/K_{AcCoA} > ^{D}V$. The use of the double-isotope fractionation test by Clark *et al.*, (24) also supported the stepwise reaction of malate synthase using $[C^2H_3\text{-methyl}]$ AcCoA and ^{13}C glyoxylate labeled at the aldehyde carbon (24). In this analysis, the addition of $[C^2H_3\text{-methyl}]$ AcCoA decreased the ^{13}C effect, indicating that $[C^2H_3\text{-methyl}]$ AcCoA increased the energy barrier of the first

step (proton abstraction from the methyl group of AcCoA) and thus decreased the KIE of the second step, bond formation with ^{13}C . Prior to these two steps, they proposed a third partially rate-limiting step that was unaffected by isotopic distribution in either substrate. The second MKIE was to determine the SKIE using $[\text{C}^2\text{H}_3\text{-methyl}] \text{AcCoA}$ in H_2O and D_2O (Figure 4D). The MKIE on $^{20}\text{V}_{[\text{C}^2\text{H}_3\text{-methyl}] \text{AcCoA}} = 1.5 \pm 0.1$ was normal, and the MKIE on $^{20}\text{V}/\text{K}_{[\text{C}^2\text{H}_3\text{-methyl}] \text{AcCoA}} = 0.6 \pm 0.1$ was inverse. The most curious feature of this result was the appearance of a non unitary, inverse $^{20}\text{V}/\text{K}$ effect with deuterated AcCoA.

Inverse solvent kinetic isotope effects are commonly attributed to proton transfer processes to groups that exhibit inverse fractionation factors. Known causes of inverse fractionation factors include the increased viscosity of D_2O than H_2O (19), metal bound waters $\sim 0.7 - 1.0$, and sulfhydryl groups, ~ 0.5 (26). The possible contribution by viscosity is unlikely given the lack of an effect on V and $\text{V}/\text{K}_{\text{AcCoA}}$ in 9% glycerol (data not shown). However, both metal bound water and sulfhydryl groups are potential sources of an inverse effect in the MS reaction. Due the position of Mg^{2+} at the end of the tube-like active site, and coordination by glyoxylate and malate, it is clear the Mg^{2+} ion serves to bind and polarize substrates, and is a central component of the reaction. Since water molecules additionally coordinate Mg^{2+} , it is a possibility that the metal bound water is the source of the inverse MKIE. Since the inverse SKIE is observed on $^{20}\text{V}/\text{K}_{\text{AcCoA}}$, solvent isotopic composition is affecting a step preceding AcCoA deprotonation and C-C bond formation and possibly the pre-catalytic partially rate-limiting step identified by Clark *et al.* (24) on the basis of the smaller intermolecular isotope effect (1.37) compared to the intramolecular primary KIE of 3.7 (27). The data does not show convincing evidence for the exact origin of the inverse MKIE. One possibility includes global solvent reorganization after the binding of substrates, allowing for a conformational change that would appropriately position the two reactants. Another alternative is that this isotope effect is due to the dehydration of the hydrated aldehyde form of glyoxylate to the aldehyde observed to coordinate Mg^{2+} and react with AcCoA.

Proposed Mechanism

The proposed mechanism starts (Scheme 2A) with the Mg^{2+} ion octahedrally coordinated by the carboxylate side chains of conserved residues Glu434 and Asp462, and four water molecules as seen in the crystal structure 1N8I (13). (Scheme 2B) As required by the inhibition studies, glyoxylate binds first displacing two of the metal-coordinated water molecules. α -Isoketovalerate, the substrate of Mg^{2+} dependent α -isopropylmalate synthase, and α -ketoglutarate, the substrate of Zn^{2+} dependent homocitrate synthase, are also positioned for the reaction by coordination to the divalent metal ion (9, 21). In MS, in Scheme 2B after the binding of AcCoA, the conserved Asp633 is the catalytic base exhibiting the pK_a value of 4.6 – 5.3, which abstracts a proton from AcCoA. This step is partially rate-limiting as evidenced by the primary deuterium kinetic isotope effect on V . In support of this, the analogous *E. coli* residue, Asp631, was mutated to Asn and exhibited no activity (22). The resulting nucleophile attacks glyoxylate to form the malyl-CoA intermediate, which we draw as the alkoxide (Scheme 2C). We propose the formation of the malyl-CoA intermediate is the first irreversible step. (Scheme 2C) The alkoxide serves to remove the proton from an adjacent metal-bound water, creating the hydroxide anion that attacks the carbonyl of the thioester intermediate. This step is the origin of ^{20}V , which requires a solvent derived proton transfer step, and in a separate step than the $[\text{C}^2\text{H}_3\text{-methyl}] \text{AcCoA}$. (Scheme 2D) The tetrahedral intermediate now decomposes with the generation of the two products. We propose Arg339 acts as a catalytic acid to protonate the leaving group, the thiolate of CoA, and is the group observed in the k_{cat} profile with a pK_b value of 9.2 ± 0.1 . In the Mtb MS-CoA-malate structure, one of the ureido nitrogens is 3.6 \AA from the thiol

of CoASH. The analogous *E. coli* residue, Arg338 was mutated to Lys and exhibited only 6.6% of WT activity (22). (Scheme 2E) The ordered release of CoA followed by L-malate completes the catalytic cycle.

Conclusions

In this work we examine Mtb malate synthase, from the currently untargeted glyoxylate shunt. We report a steady-state ordered bi bi kinetic mechanism. Additionally, we propose a Mg^{2+} centered reaction mechanism in which glyoxylate binds first to the enzyme, coordinating Mg^{2+} . Asp633 acts as a catalytic base to abstract a proton from AcCoA, generating a nucleophilic attack on glyoxylate to form a malyl-CoA intermediate. A water proton is abstracted by the intermediate alkoxide, which generates a hydroxyl nucleophile that attacks the malyl-CoA intermediate. Arg339 protonates the CoA, prompting the decomposition of the tetrahedral intermediate, and the ordered release of the products CoA and malate complete the catalytic sequence. The new kinetic and chemical mechanistic data could support inhibitor design for malate synthase, and thus target the glyoxylate shunt and persistence in Mtb.

Supplementary Material

Refer to Web version on PubMed Central for supplementary material.

Acknowledgments

This work was supported by the National Institutes of Health Grant AI33696 to J.S.B. and T32 AI007501 to C.E.Q.

We thank Dr. Hua Xu for his assistance with the synthesis of dethio-CoA and $[C^2H_3]$ AcCoA, Edward Nieves for performing the mass spectrometry, Dr. Subray Hegde for his assistance in the cloning and purification of WT MS, and Clarissa Czekster and An Vandemeulebroucke for their insightful discussions.

Abbreviations

AcCoA	acetyl coenzyme A
α-IPMS	α -isopropylmalate synthase
CoA	coenzyme A
CS	citrate synthase
DDT	dithiothreitol
DMF	N,N-dimethylformamide
DTP	4,4'-dithiodipyridine
<i>E. coli</i>	<i>Escherichia coli</i>
EDTA	ethylenediaminetetraacetic acid
E_t	total enzyme
gly	glyoxylate
HCS	homocitrate synthase
HEPES	N-(2-hydroxyethyl)piperazine-N'-(2-ethanesulfonic acid)
IPTG	isopropyl β -D-thiogalactopyranoside
KIE	kinetic isotope effect

LB	Luria broth
MES	2-(N-morpholino)ethanesulfonic acid
MS	malate synthase
Mtb	<i>Mycobacterium tuberculosis</i>
MDR	multidrug resistant
MKIE	multiple kinetic isotope effect
Ni-NTA	nickel nitriloacetic acid
PCR	polymerase chain reaction
SDS-PAGE	sodium dodecyl sulfate-polyacrylamide gel electrophoresis
SKIE	solvent kinetic isotope effect
TAPS	N-[tris(hydroxymethyl)methyl]-3-aminopropanesulfonic acid
TCA	tricarboxylic acid
Tris	tris(hydroxymethyl)aminomethane
TEA	triethylamine
TFA	trifluoroacetic acid
WT	wild type
XDR	extensively drug resistant

References

- Dunn MF, Ramirez-Trujillo JA, Hernandez-Lucas I. Major roles of isocitrate lyase and malate synthase in bacterial and fungal pathogenesis. *Microbiology*. 2009; 155:3166–3175. [PubMed: 19684068]
- Kondrashov FA, Koonin EV, Morgunov IG, Finogenova TV, Kondrashova MN. Evolution of glyoxylate cycle enzymes in Metazoa: evidence of multiple horizontal transfer events and pseudogene formation. *Biol Direct*. 2006; 1:31. [PubMed: 17059607]
- Wayne LG, Sohaskey CD. Nonreplicating persistence of mycobacterium tuberculosis. *Annual review of microbiology*. 2001; 55:139–163.
- Wayne LG, Lin KY. Glyoxylate metabolism and adaptation of *Mycobacterium tuberculosis* to survival under anaerobic conditions. *Infection and immunity*. 1982; 37:1042–1049. [PubMed: 6813266]
- McKinney JD, Honer zu Bentrup K, Munoz-Elias EJ, Miczak A, Chen B, Chan WT, Swenson D, Sacchettini JC, Jacobs WR Jr, Russell DG. Persistence of *Mycobacterium tuberculosis* in macrophages and mice requires the glyoxylate shunt enzyme isocitrate lyase. *Nature*. 2000; 406:735–738. [PubMed: 10963599]
- WHO. 2010/2011 Tuberculosis Global Facts. March 11. 2011
http://www.who.int/tb/publications/2010/factsheet_tb_2010.pdf
- Manabe YC, Bishai WR. Latent *Mycobacterium tuberculosis*-persistence, patience, and winning by waiting. *Nature medicine*. 2000; 6:1327–1329.
- Heath RJ, Rock CO. The Claisen condensation in biology. *Natural product reports*. 2002; 19:581–596. [PubMed: 12430724]
- de Carvalho LP, Blanchard JS. Kinetic and chemical mechanism of alpha-isopropylmalate synthase from *Mycobacterium tuberculosis*. *Biochemistry*. 2006; 45:8988–8999. [PubMed: 16846242]
- Andi B, West AH, Cook PF. Kinetic mechanism of histidine-tagged homocitrate synthase from *Saccharomyces cerevisiae*. *Biochemistry*. 2004; 43:11790–11795. [PubMed: 15362863]

11. Kurz LC, Drysdale G, Riley M, Tomar MA, Chen J, Russell RJ, Danson MJ. Kinetics and mechanism of the citrate synthase from the thermophilic archaeon *Thermoplasma acidophilum*. *Biochemistry*. 2000; 39:2283–2296. [PubMed: 10694395]
12. de Carvalho LP, Blanchard JS. Kinetic analysis of the effects of monovalent cations and divalent metals on the activity of *Mycobacterium tuberculosis* alpha-isopropylmalate synthase. *Archives of biochemistry and biophysics*. 2006; 451:141–148. [PubMed: 16684501]
13. Smith CV, Huang CC, Miczak A, Russell DG, Sacchettini JC, Honer zu Bentrup K. Biochemical and structural studies of malate synthase from *Mycobacterium tuberculosis*. *J Biol Chem*. 2003; 278:1735–1743. [PubMed: 12393860]
14. Remington SJ. Structure and mechanism of citrate synthase. *Current topics in cellular regulation*. 1992; 33:209–229. [PubMed: 1499334]
15. ProtParam Tool. August 19. 2010 <http://ca.expasy.org/tools/protparam.html>
16. Pace CN, Vajdos F, Fee L, Grimsley G, Gray T. How to measure and predict the molar absorption coefficient of a protein. *Protein Sci*. 1995; 4:2411–2423. [PubMed: 8563639]
17. Chase JF, Middleton B, Tubbs PK. A coenzyme A analogue, desulpho-coA; preparation and effects on various enzymes. *Biochem Biophys Res Commun*. 1966; 23:208–213. [PubMed: 5928913]
18. Wilson IB. Preparation of acetyl coenzyme A1. *Journal of the American Chemical Society*. 1952; 74:3205–3206.
19. Karsten WE, Lai CJ, Cook PF. Inverse Solvent Isotope Effects in the NAD-Malic Enzyme Reaction Are the Result of the Viscosity Difference between D2O and H2O: Implications for Solvent Isotope Effect Studies. *Journal of the American Chemical Society*. 1995; 117:5914–5918.
20. Durchschlag H, Biedermann G, Eggerer H. Large-scale purification and some properties of malate synthase from baker's yeast. *Eur J Biochem*. 1981; 114:255–262. [PubMed: 7011808]
21. Qian J, West AH, Cook PF. Acid-base chemical mechanism of homocitrate synthase from *Saccharomyces cerevisiae*. *Biochemistry*. 2006; 45:12136–12143. [PubMed: 17002313]
22. Anstrom DM, Kallio K, Remington SJ. Structure of the *Escherichia coli* malate synthase G:pyruvate:acetyl-coenzyme A abortive ternary complex at 1.95 Å resolution. *Protein science: a publication of the Protein Society*. 2003; 12:1822–1832. [PubMed: 12930982]
23. Howard BR, Endrizzi JA, Remington SJ. Crystal structure of *Escherichia coli* malate synthase G complexed with magnesium and glyoxylate at 2.0 Å resolution: mechanistic implications. *Biochemistry*. 2000; 39:3156–3168. [PubMed: 10715138]
24. Clark JD, O'Keefe SJ, Knowles JR. Malate synthase: proof of a stepwise Claisen condensation using the double-isotope fractionation test. *Biochemistry*. 1988; 27:5961–5971. [PubMed: 2847778]
25. Hermes JD, Roeske CA, O'Leary MH, Cleland WW. Use of multiple isotope effects to determine enzyme mechanisms and intrinsic isotope effects. Malic enzyme and glucose-6-phosphate dehydrogenase. *Biochemistry*. 1982; 21:5106–5114. [PubMed: 7138850]
26. Quinn, DM.; Sutton, LD. Theoretical Basis and Mechanistic Utility of Solvent Isotope Effects. In: Cook, PF., editor. *Enzyme Mechanism from Isotope Effects*. CRC Press; Boca Raton, FL: 1991. p. 115-116.
27. Lenz H, Eggerer H. Enzymic generation of chiral acetates. A quantitative evaluation of their configurational assay. *Eur J Biochem*. 1976; 65:237–246. [PubMed: 1278179]

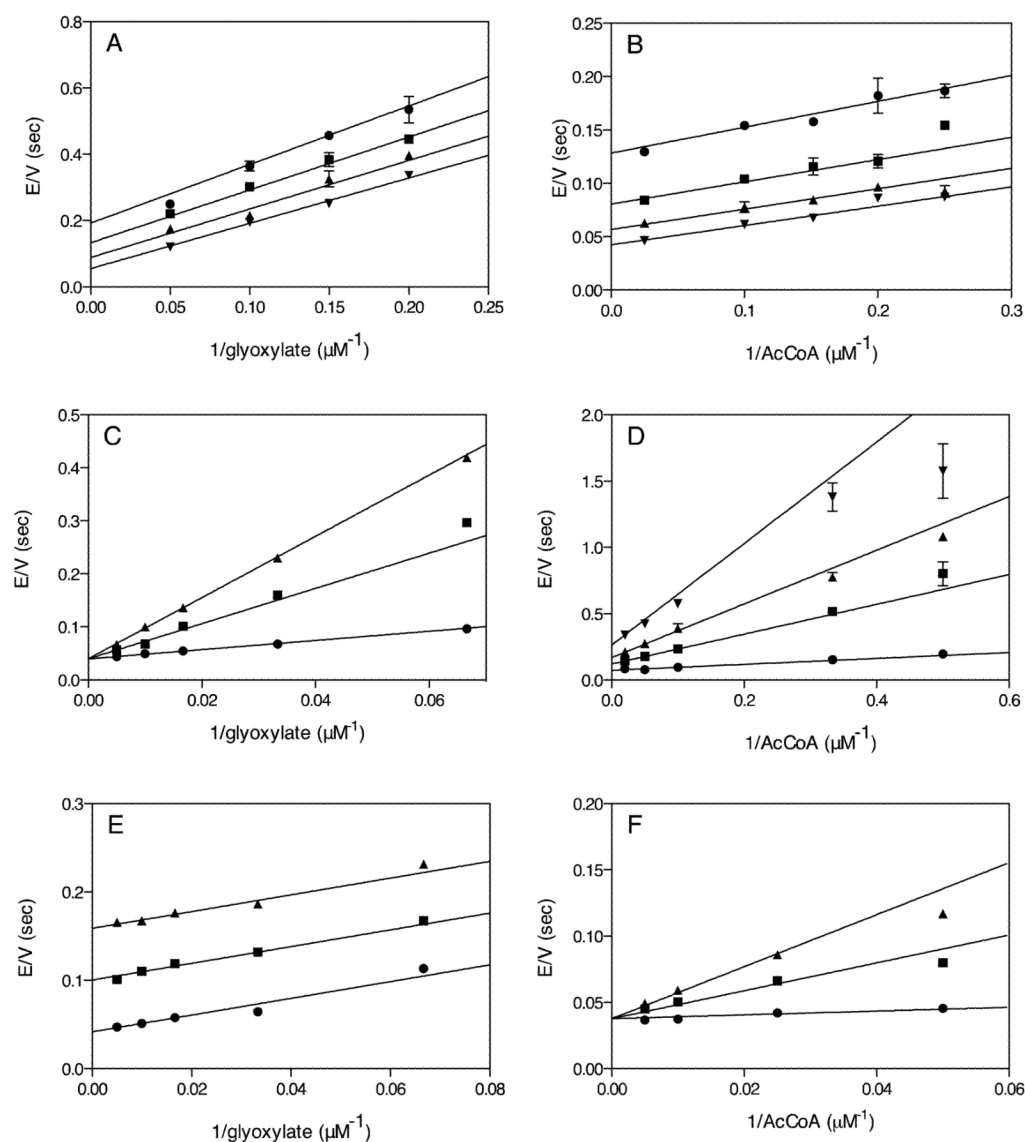
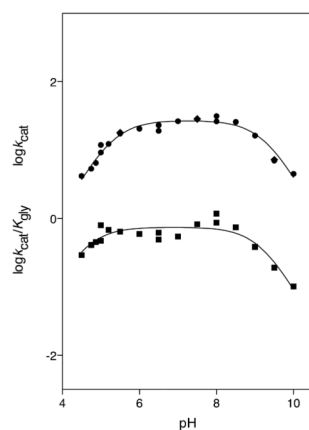


FIGURE 1. “Elucidation of the Kinetic Mechanism of C619S MS.” (A) Initial velocity at varying concentrations of glyoxylate (5 – 20 μM) and different fixed concentrations of AcCoA: 3 μM (\bullet), 5 μM (\blacksquare), 10 μM (\blacktriangle), 40 μM (\blacktriangledown). Eq 2 determined $k_{\text{cat}} = 23 \pm 3 \text{ sec}^{-1}$, $K_{\text{gly}} = 30 \pm 6 \mu\text{M}$, $K_{\text{AcCoA}} = 10 \pm 3 \mu\text{M}$, $K_{\text{ia}} = 3 \pm 2 \mu\text{M}$. (B) Initial velocity at varying concentrations of AcCoA (4 – 40 μM) and different fixed concentrations of glyoxylate: 10 μM (\bullet), 20 μM (\blacksquare), 40 μM (\blacktriangle), 100 μM (\blacktriangledown). Global fitting to eq 2 which determined $k_{\text{cat}} = 30 \pm 2 \text{ sec}^{-1}$, $K_{\text{gly}} = 29 \pm 4 \mu\text{M}$, $K_{\text{AcCoA}} = 5 \pm 1 \mu\text{M}$, $K_{\text{ia}} = 0.7 \pm 0.7 \mu\text{M}$. (C) Product inhibition by malate with 25 μM AcCoA and 15–200 μM glyoxylate at different fixed concentrations of malate: 0 mM (\bullet), 25 mM (\blacksquare), 50 mM (\blacktriangle). Global fitting to eq 4 determined the inhibition constant, $K_{\text{is}} = 9 \pm 1 \text{ mM}$. (D) Product inhibition by malate with 30 μM glyoxylate and 2 – 50 μM AcCoA at different fixed concentrations of malate: 0 mM (\bullet), 25 mM (\blacksquare), 50 mM (\blacktriangle), 100 mM (\blacktriangledown). Global fitting of to eq 6 determined $K_{\text{is}} = 6 \pm 1 \text{ mM}$ and $K_{\text{ji}} = 38 \pm 7 \text{ mM}$. (E) Dead-end inhibition by dethio-AcCoA with 25 μM AcCoA and 15–200 μM glyoxylate and different fixed concentrations of dethio-AcCoA: 0 μM (\bullet), 25 μM (\blacksquare), 50 μM (\blacktriangle). Global fitting to eq 5 determined the inhibition constant $K_{\text{ji}} = 18 \pm 1 \mu\text{M}$ (F) Dead-end inhibition with 300 μM

glyoxylate and 20 – 200 μM AcCoA and different fixed concentrations of dethio-AcCoA: 0 μM (●), 25 μM (■), 50 μM (▲). Global fitting to eq 4 determined $K_{is} = 4 \pm 1 \mu\text{M}$.

**FIGURE 2.**

“pH dependence of C619 MS.” k_{cat} determined at saturating AcCoA and varying glyoxylate (●). Fitting to eq 3 determined $\text{p}K_{\text{a}} = 5.3 \pm 0.1$ and $\text{p}K_{\text{b}} = 9.2 \pm 0.1$. Superimposed (◆) are saturating glyoxylate and varied AcCoA from the control reactions in the pH dependence of the KIEs. $k_{\text{cat}}/K_{\text{gly}}$ is represented by (■) where global fitting to eq 3 gave $\text{p}K_{\text{a}} = 4.6 \pm 0.2$ and $\text{p}K_{\text{b}} = 9.1 \pm 0.3$.

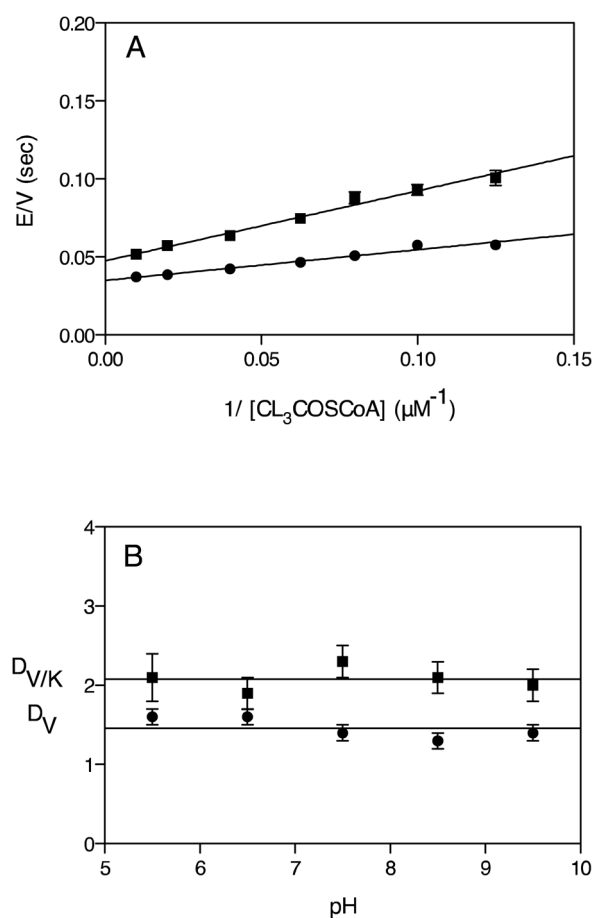
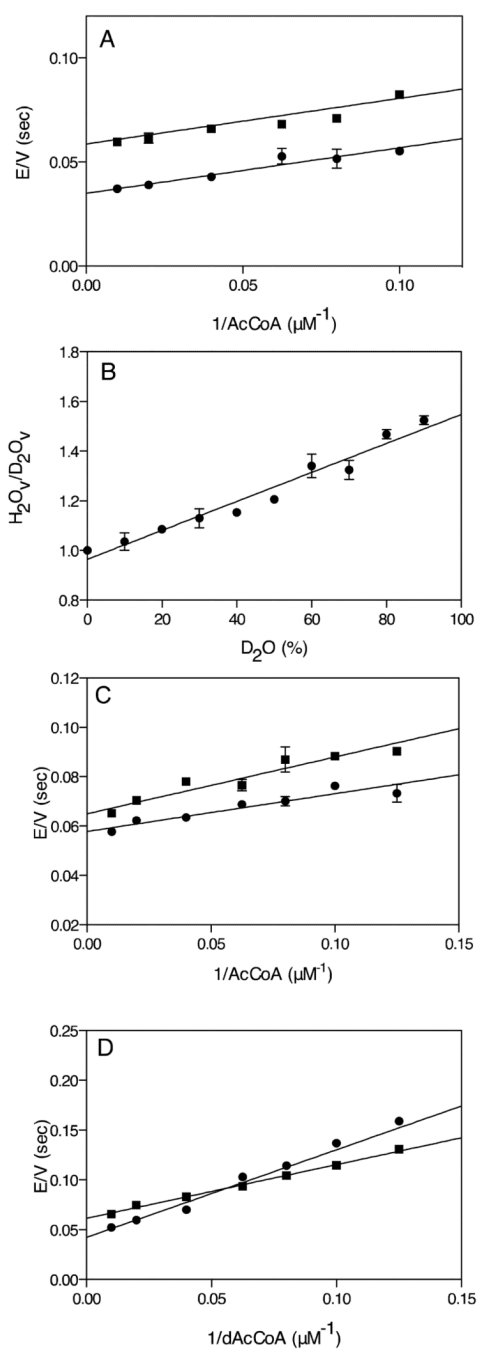
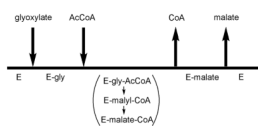


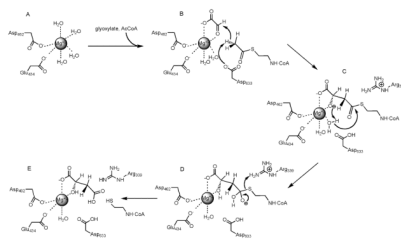
FIGURE 3. “Kinetic isotope effects utilizing deuterated AcCoA.” (A) KIEs at saturating glyoxylate (300 μM) and varying (8–100 μM) AcCoA, where L = H (●) or deuterated AcCoA (■) at pH 7.5, $D_V = 1.4 \pm 0.1$ and $D_V/K_{AcCoA} = 2.3 \pm 0.3$ where L = D. (B) D_V and D_V/K_{AcCoA} were determined in an identical method to Fig. 3A at 1 pH unit increments from 5.5 – 9.5. The lack of pH dependence was fit with the lines $D_V = 1.46$ and $D_V/K_{AcCoA} = 2.08$, the average of the respective KIEs from each pH.

**FIGURE 4.**

“Solvent kinetic isotope effects in D₂O.” (A) SKIEs at saturating glyoxylate (300 μM) and varying AcCoA (10–100 μM) at pH 7.5 in H₂O (●) or 93% D₂O (■), $D_2O_V = 1.7 \pm 0.1$ and $D_2O_V/K_{AcCoA} = 1.0 \pm 0.3$. (B) Proton inventory at saturating glyoxylate (300 μM) and saturating AcCoA (100 μM) at pH 7.5 in 10% D₂O increments from 0–90%. (C) Multiple kinetic isotope effects using saturating glyoxylate (300 μM) and varying deuterated AcCoA (8–100 μM) (■) or AcCoA (●) in D₂O, $D_2O_V_{[C2H3\text{-methyl}] AcCoA} = 1.1 \pm 0.1$ and $D_2O_V/K_{[C2H3\text{-methyl}] AcCoA} = 1.5 \pm 0.3$. (D) Multiple kinetic isotope effects using saturating glyoxylate (300 μM) and varying deuterated AcCoA (8–100 μM) in H₂O (●) and D₂O (■), $D_2O_V_{[C2H3\text{-methyl}] AcCoA} = 1.5 \pm 0.1$ and $D_2O_V/K_{[C2H3\text{-methyl}] AcCoA} = 0.6 \pm 0.1$.



Scheme 1.
 Ordered Bi Bi Kinetic Mechanism of Malate Synthase



Scheme 2.
Proposed Chemical Mechanism of Malate Synthase